Check for updates

Nanomagnetic tetraaza (N₄ donor) macrocyclic Schiff base complex of copper(II): synthesis, characterizations, and its catalytic application in Click reactions†

Masoomeh Norouzi,* Nasim Noormoradi and Masoud Mohammadi [ID]

In this research, a novel nanomagnetic tetra-azamacrocyclic Schiff base complex of copper(II) was produced *via* a post-synthetic surface modification of an Fe_3O_4 surface by a silane-coupling agent that contains acetylacetone functionalities at the end of its chain. Moreover, the target Cu complex that involves a tetradentate Schiff base ligand was obtained from a template reaction with *o*-phenylenediamine and $Cu(NO_3)_2 \cdot 3H_2O$. Furthermore, the prepared complex was nominated as [Fe_3O_4@TAM-Schiff-base-Cu(II)]. The Fourier-transform infrared (FT-IR) analysis indicates the presence of a Schiff-base-Cu complex in the catalyst. X-ray spectroscopy (EDS) and TGA analysis reveal that approximately 6−7% of the target catalyst comprises hydrocarbon moieties. The scanning electron microscope (SEM) and transmission electron microscopy (TEM) images demonstrate the presence of uniformly shaped particles, nearly spherical in nature, with sizes ranging from 9 to 18 nm. [Fe_3O_4@TAM-Schiff-base-Cu(II)] was applied as a catalyst for the click synthesis of a diverse range of 5-substituted-1*H*-tetrazoles in PEG-400 as a green medium. Regarding the electrical properties of the Cu(II) complex, the presence of a tetra-aza (N₄ donor) macrocyclic Schiff base as an N-rich ligand was reasonable – leading to its excellent capacity to catalyze these organic transformations. Finally, the high magnetization value (44.92 emu g⁻¹) of [Fe_3O_4@TAM-Schiff-base-Cu(II)] enables its recycling at least four times without compromising the catalytic efficiency.

Introduction

Many types of biological functions have been attributed to heterocyclic molecules.[1,2] Moreover, five-membered N-containing heterocyclic molecules are dominant in the field of medicinal chemistry.[3,4] Azole moieties are a type of synthetic chemical molecule that is not found in nature.[5] Tetrazoles, which were first synthesized by J. A. Bladin in 1885, are made of a doubly unsaturated five-membered ring containing four nitrogen atoms and one carbon atom, known as the greatest quantity of nitrogen that may be found in a stable heterocyclic ring.[6,7] It is possible for these compounds to exist in a wide variety of tautomeric forms, as well as anions and cations, such as mono- and di-substituted NH tetrazole derivatives.[8] In this regard, recent reviews have shown that tetrazole-containing molecules can be prepared from the catalytic reactions of amines, amides, aldoximes, aldehydes, and nitriles.[9–15] The most common method is to react sodium azide as the nitrogen

source with nitriles in the presence of a transition metal catalyst.[16] Recently, chemists have focused on developing an efficient catalytic synthesis of 5-substituted tetrazoles through this approach.[14,17–20] However, there is still a lot to learn about these adaptable substances, and further research is needed to achieve the best catalytic method under green conditions.

Homogeneous catalysts, which have been widely utilized to catalyze chemical processes, have low recoverability, reusability, and stability.[17] To circumvent these constraints, heterogeneous catalysts that are more efficient and environmentally benign are being investigated.[21,22] Several investigations have been carried out in which supported precious metals, such as palladium, gold and silver, were utilized as catalysts for the click functionalization of aryl nitriles to their corresponding 5-substituted-1*H*-tetrazoles (RCN₄H). Generally, the immobilization of transition metals on high-surface-area materials, such as nanomaterials, has been documented.[17,23,24] However, these heterogenized catalysts suffer from sluggish reaction rates and severe mass-transfer limitations, in addition to active species leaching during reactions. Recently, it has been demonstrated that modifying and functionalizing nanomaterials with organic ligands and complexes *via* covalent or noncovalent interactions is an alternative and efficient method to produce hybrid catalysts.[25,26]

Department of Chemistry, Faculty of Science, Ilam University, P.O. Box 69315516, Ilam, Iran. E-mail: m.norozi@ilam.ac.ir

† Electronic supplementary information (ESI) available. See DOI: https://doi.org/10.1039/d3na00580a

When one aims at changing the size, spatial organization and electronic configuration, nanocatalysts are alluring alternatives to the conventional catalyst.[25,27–29] Notably, they have a high surface-to-volume ratio and improved catalytic activity, selectivity, and stability.[30,31] The filtration or centrifugation processes used to separate and recover nanocatalysts are difficult and ineffective, which is made worse by the nanoscale size of the catalyst particles, endangering their viability and economics.[17,32] Due to their ease of separation from the reaction medium by means of an external magnetic field, magnetic nanoparticles (MNPs) appear to be a viable solution to these problems.[33–35]

Recently, Schiff-base transition metal complexes have piqued the interest of researchers due to their structural characteristics, such as ligand stiffness, donor atom type, and catalytic uses.[36,37] These transition metal complexes of Schiff bases are good organic synthesis agents.[38–40] Since these structural units are engaged in a number of catalytic, biological, and industrial activities, tremendous development in the chemistry of tetraazamacrocyclic complexes has been observed.[41–44] In this sense, the present work aims at using acetylacetone (acac) as a versatile carbonyl synthon to combine with o-phenylenediamine in order to make an acac-based tetraaza (N_4 donor) macrocyclic Schiff base as a new heterodentate ligand.

Herein, Fe_3O_4 is used as a support material for the ACAC functionalities. Afterwards, the corresponding $Cu^{(II)}$ Schiff base complex was synthesized using the template approach, and then it was applied as a promoter to assist the sustainable synthesis of 5-substituted-1H-tetrazole derivatives in PEG-400 as a greener alternative to the traditional solvents. According to the findings, the [Fe_3O_4@TAM-Schiff-base-$Cu^{(II)}$] complex possesses greater performance and reusability in comparison to those of the majority of reported transformations.

Experimental

Materials and methods

All of the materials used in this work were purchased from the Merck and Aldrich companies and used without purification. FTIR analysis (FTIR, USA, PerkinElmer, 400–4000 cm^{-1}) was utilized for the identification of functional group compositions. The examination of XRD patterns was conducted within the range of 2 = 10–80° (1.5405 A0 = XRD-BRUKER) to determine the crystallography of the nanoparticles. Thermogravimetric analysis was performed using an STA503 instrument (Germany, BAHR) in a temperature range of 35 °C to 805 °C, with a rising rate of 10 °C min^{-1} and an air atmosphere. Elemental components and their distribution patterns were determined through EDX/mapping analysis (VEGA II Detector, TESCAN, Czech Republic). The surface morphology of the catalyst was examined using FESEM (FESEM/TE/SCAN, Philips) and TEM (TEM/CM 120, Philips) analysis. Magnetic characteristics of the nanocatalyst were measured using a vibrating sample magnetometer (VSM, model EZ-9, G. Colombo 81, 20133 Milano, Italy). The specific surface area of the samples was determined using the BET (Brunauer–Emmett–Teller) method with a Micromeritics ASAP 2020 instrument. Nitrogen adsorption measurements were performed at 77 K after degassing the samples at 100 °C under vacuum for 2

hours. The relative pressure (P/P_0) range for the measurements was set between 0.03 and 0.99. The instrument was calibrated using standard reference materials prior to the measurements. Data analysis was conducted using the BET equation and the surface area was calculated based on the adsorption isotherm.

Preparation of the [Fe_3O_4@TAM-Schiff-base-$Cu^{(II)}$] complex

During the first step, Fe_3O_4 and 3-(3-trimethoxysilylpropyl)acetylacetone were prepared according to previous methods.[45,46] Afterwards, in order to synthesize the target Fe_3O_4@SiO_2@sil-acac MNPs, 1 g of Fe_3O_4 MNPs was dispersed in 50 mL of toluene for 30 min, and then 5 mmol of 3-(3-trimethoxysilylpropyl)acetylacetone was added to the reaction mixture and stirred under reflux conditions for 24 h. Subsequently, the obtained particles were separated using an external magnet, washed with ethanol and acetone, and dried at 60 °C. At the final step, the [Fe_3O_4@TAM-Schiff-base-$Cu^{(II)}$] complex was prepared via a template reaction. In this sense, 1 g of Fe_3O_4@SiO_2@sil-acac MNPs was dispersed in 50 mL of ethanol for 30 min, and then 2.5 mmol of o-phenylenediamine and 2.5 mmol of $Cu(NO_3)_2 \cdot 3H_2O$ were added to the reaction mixture and stirred under a N_2 atmosphere at 80 °C for 1 day. Afterwards, the obtained [Fe_3O_4@TAM-Schiff-base-$Cu^{(II)}$] complex was separated using an external magnet, washed with water and ethanol, and dried at room temperature (Scheme 1).

General procedure for the synthesis of 5-substituted 1H-tetrazoles over the catalysis of a [Fe_3O_4@TAM-Schiff-base-$Cu^{(II)}$] complex

A round-bottomed flask containing one milliliter of PEG-400 was used to combine a mixture – consisting of 25 mg of the [Fe_3O_4@TAM-Schiff-base-$Cu^{(II)}$] complex, 1.4 mmol of sodium azide, and 1.0 mmol of aryl nitrile. Eventually, the reaction mixture was agitated at a temperature of 120 °C. After reaction completion (controlled via TLC) and a simple work-up, involving magnetic decantation of the catalyst from the diluted mixture, extraction with ethyl acetate, washing, drying and solvent evaporation, the crude products were purified using a silica gel plate.
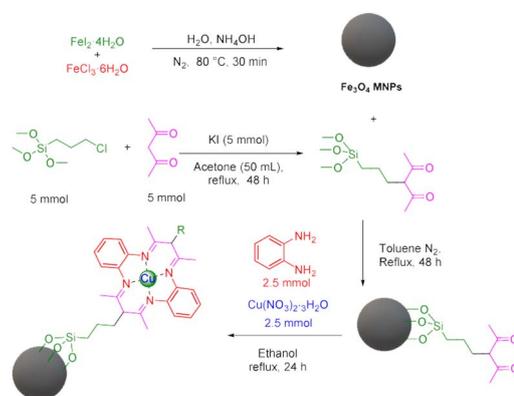
Scheme 1 Stepwise synthesis of [Fe_3O_4@TAM-Schiff-base-$Cu^{(II)}$] complex.

Spectral data

5-Phenyltetrazole (Table 2, entry 1). ^{1}H NMR (400 MHz, DMSO-d_6), δ (ppm):16.92 (s, 1H), 8.03 (dd, $J = 6.5$, 3.3 Hz, 2H), 7.60 (dd, $J = 5.1$, 2.1 Hz, 3H).

5-p-Tolyl-1H-tetrazole (Table 2, entry 2). ^{1}H NMR (400 MHz, DMSO-d_6), δ (ppm): 16.68 (s, 1H), 7.93–7.89 (d, $J = 8$ Hz, 2H), 7.42–7.38 (d, $J = 8$ Hz, 2H), 2.38 (s, 3H).

5-(4-Trifluoromethyl-phenyl)-1H-tetrazole (Table 2, entry 3). ^{1}H NMR (400 MHz, DMSO-d_6), δ (ppm): 8.35–8.33 (d, $J = 8$ Hz, 2H), 7.98–7.95 (d, $J = 8$ Hz, 1H), 7.88–7.83 (t, 1H).

5-(4-Nitrophenyl)tetrazole (Table 2, entry 5). ^{1}H NMR (400 MHz, DMSO-d_6), δ (ppm): 8.46–8.81 (d, $J = 8$ Hz, 2H), 8.52–8.33 (m, 2H).

5-(2-Fluoro-phenyl)-1H-tetrazole (Table 2, entry 6). ^{1}H NMR (400 MHz, DMSO-d_6), δ (ppm): 16.86 (b, 1H (N–H)), 8.07 (s, 1H), 7.67–7.64 (d, $J = 8$ Hz, 1H), 7.52–7.41 (m, 2H).

5-(2-Chlorophenyl)tetrazole (Table 2, entry 7). ^{1}H NMR (400 MHz, DMSO-d_6), δ (ppm): 16.88 (b, 1H (N–H)), 8.01 (s, 1H), 7.82–7.79 (d, $J = 8$ Hz, 1H), 7.73–7.72 (d, $J = 8$ Hz, 1H), 7.63–7.55 (m, 1H).

5-(4-Chloro-phenyl)-1H-tetrazole (Table 2, entry 8)

^{1}H NMR (400 MHz, DMSO-d_6), δ (ppm): 16.89 (b, 1H (N–H), 8.07 (s, 1H), 8.05–8.02 (d, $J = 8$ Hz, 2H), 7.70–7.66 (d, $J = 8$ Hz, 2H).

5-(4-Bromo-phenyl)-1H-tetrazole (Table 2, entry 9). ^{1}H NMR (400 MHz, DMSO-d_6), δ (ppm): 7.98–7.95 (d, $J = 8$ Hz, 2H), 7.83–7.80 (d, $J = 8$ Hz, 2H).

4-(1H-Tetrazol-5-yl)-phenol (Table 2, entry 11). ^{1}H NMR (400 MHz, DMSO-d_6), δ (ppm): 10 (br, 1H, OH), 7.86–7.83 (d, $J = 8$ Hz, 2H), 6.95–6.98 (d, $J = 8$ Hz, 2H).

2-(1H-Tetrazol-5-yl)-benzonitrile (Table 2, entry 12). ^{1}H NMR (400 MHz, DMSO-d_6), δ (ppm): 8.19–8.06 (m, 2H), 7.95–7.90 (t, $J = 8$ Hz, 1H), 7.80–7.75 (t, $J = 8$ Hz, 1H).

Results and discussion

Catalyst characterization

The successful synthesis of target nanomaterials was confirmed by the investigation of their functional groups, crystalline phases, thermal stability, elemental composition, surface size and morphologies, and magnetic properties *via* analytical techniques.

Fourier-transform infrared spectroscopy (FTIR)

The spectra of Fe_3O_4 and $Fe_3O_4@SiO_2@sil$-acac are exactly the same as said in earlier reports regarding the fingerprints of the samples.[45] A prominent –OH stretching absorption band was detected in the FT-IR spectrum of Fe_3O_4 (Fig. 1a) in the range of 3055–3640 cm^{-1}. The stretching vibration mode of the Fe–O bonds causes peaks at 580 cm^{-1} and 630 cm^{-1}.[47] The FT-IR spectra of 3-(3-trimethoxysilylpropyl)acetylacetone functionalized Fe_3O_4 show the appearance of bands between 2918 cm^{-1} and 2858 cm^{-1} that are the result of C–H stretching vibrations in the CH_2 groups (Fig. 1b).[48] Moreover, strong signals at 1703 cm^{-1} are attributed to the stretching vibration of C=O groups, indicating that the ligand was grafted on Fe_3O_4 nanoparticles.[49] Regarding the [$Fe_3O_4@TAM$-Schiff-base-Cu$^{(II)}$] complex, the imine bond (C=N) and C–N stretching vibrations are accountable for the bands that appear at

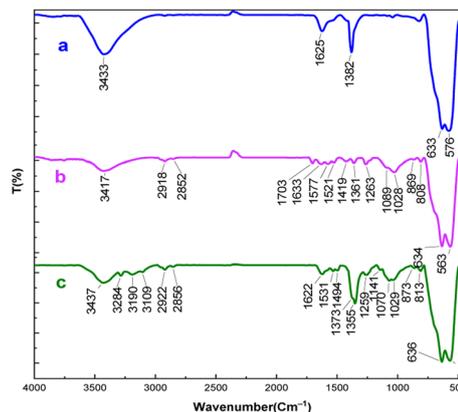Fig. 1 FT-IR spectra of (a) Fe_3O_4, (b) $Fe_3O_4@SiO_2@sil$-acac, (c) the [$Fe_3O_4@TAM$-Schiff-base-Cu$^{(II)}$] complex.
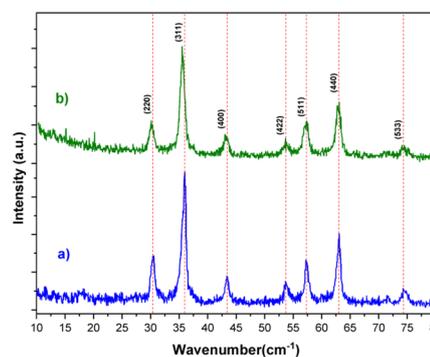

Fig. 2 XRD pattern of (a) Fe_3O_4 and (b) [$Fe_3O_4@TAM$-Schiff-base-Cu$^{(II)}$] complex.

1622 cm^{-1} and 1170 cm^{-1}, respectively (Fig. 1c).[48,50] In addition, the aromatic C–H groups, aromatic-N stretching vibration and aromatic C–C bonds are responsible for the bands that appear at 2981 cm^{-1}, 1355 cm^{-1} and 1494 cm^{-1}, respectively.[51] Furthermore, the disparagement of C=O groups and the formation of imine (C=N) and C–N bands indicated the production of the target Cu(II)-Schiff base complex through the template reaction.

Powder X-ray diffraction (PXRD)

The XRD spectra of the bare Fe_3O_4 and [$Fe_3O_4@TAM$-Schiff-base-Cu$^{(II)}$] complex are depicted in Fig. 2. Crystalline Fe_3O_4 MNPs are accountable for the sharp peaks at $2\theta = 30.16°$, 35.59°, 43.19°, 53.70°, 57.32°, 63.03° and 74.44°, corresponding to the reflection planes (220), (311), (400), (422), (511), (440) and (533), respectively (JCPDS card no. 34-421).[52,53] Thus, it is possible to conclude that the magnetic Fe_3O_4 phase was maintained even when the functionalization process was performed. The results confirm the successful formation of the [TAM-Schiff-base-Cu$^{(II)}$] complex over the surface of Fe_3O_4 MNPs.

Thermogravimetric analysis (TGA) and derivative thermogravimetry (DTG)

The DTG-TGA method was used to evaluate the mass ratios and thermal stability of the [$Fe_3O_4@TAM$-Schiff-base-Cu$^{(II)}$]

complex. Furthermore, multiple degradation stages are depicted in Fig. 3. The evaporation of moisture, water and organic solvents that are physically adsorbed on the prepared nanocomposite caused the two initial weight losses of 2.66% below 160 °C.[54] Disintegration of the supported Schiff base–copper complex causes the next weight loss in the range of 162–400 °C, which is about 6.78%. Significantly, DTG max was detected at 335.69 °C. The physical changes, such as fusion, dehydration reactions and phase crystalline change (oxidation of Fe_3O_4 to Fe_2O_3 (hematite) and the formation of SiO_2 metal oxide), are the causes of the two weight gains in the temperature range of 400 to 648 °C. According to the TGA-DTG results, the [Fe_3O_4@TAM-Schiff-base-Cu$^{(II)}$] complex has an excellent thermal stability, which is an efficient characteristic for catalysis at high temperatures.

Energy-dispersive X-ray spectroscopy (EDAX) and inductively coupled plasma optical emission spectroscopy (ICP-OES)

The EDAX analysis confirmed the presence of all the expected elements in the [Fe_3O_4@TAM-Schiff-base-Cu$^{(II)}$] complex composition. As shown in Fig. 4, the presence of iron and oxygen peaks refers to key elements of the Fe_3O_4 MNPs. In addition, the presence of a silicon peak affirms the successful grafting of the 3-(3-trimethoxysilylpropyl)acetylacetone on Fe_3O_4 and the construction of Fe_3O_4@SiO_2@sil-acac MNPs. As shown in Fig. 4, the presence of key elements, such as carbon, nitrogen, and copper, affirms that the template reaction of Fe_3O_4@SiO_2@sil-acac MNPs with *o*-phenylenediamine and copper salt leads to the successful formation of the target Cu(II) Schiff base complex. Furthermore, the exact amount of copper in the [Fe_3O_4@TAM-Schiff-base-Cu$^{(II)}$] complex was determined to be 0.076 mmol g^{-1} through the utilization of ICP-OES methodology.

Wavelength dispersive X-ray analysis (WDS)

The elemental mapping analysis of the [Fe_3O_4@TAM-Schiff-base-Cu$^{(II)}$] complex is shown in Fig. 5. The obtained mapping images indicate the high density of iron and oxygen elements that come from the catalyst support, which, based on thermal analysis, constitute more than 90% of the sample. In addition, the mapping images indicate that the silicon, carbon, nitrogen, and
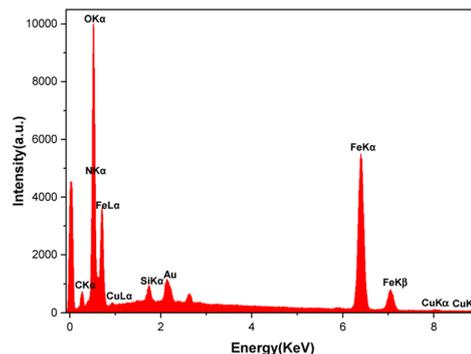
Fig. 4 EDAX analysis of the [Fe_3O_4@TAM-Schiff-base-Cu$^{(II)}$] complex.

copper moieties are excellently distributed on the Fe_3O_4 support. As can be seen in these photograms, there is a good agreement between the distribution patterns of these elements, which demonstrated that the imine groups of the TAM-Schiff-base ligand serve as donor nitrogen atoms for the coordination of Cu(II) ions. The uniform dispersion of copper as the active component in this heterogeneous catalyst is expected to result in an increase in the number of active sites. This, in turn, is anticipated to enhance the accessibility of reactants and, consequently, lead to a higher production rate of organic products.

Scanning electron microscopy (SEM)

As displayed in Fig. 6, SEM-derived images are provided to investigate the topographical characteristics of the [Fe_3O_4@TAM-Schiff-base-Cu$^{(II)}$] complex. The morphological study showed that the catalyst was made up of uniform particles that were almost sphere-like in shape. These particles are made up of small particles that are slightly agglomerated and have a particle size of less than 50 nm, which, due to the formation of catalytic layers on its surface is slightly larger than the particle size of Fe_3O_4 found in the literature,[55] Moreover, the SEM micrograph revealed the successful immobilization of the [TAM-Schiff-base-Cu$^{(II)}$] complex on the Fe_3O_4 surface, while the catalytic support retained its spherical morphology upon modification.

Transmission electron microscopy (TEM)

The morphology of the [Fe_3O_4@TAM-Schiff-base-Cu$^{(II)}$] complex was observed using TEM. The results present well-dispersed
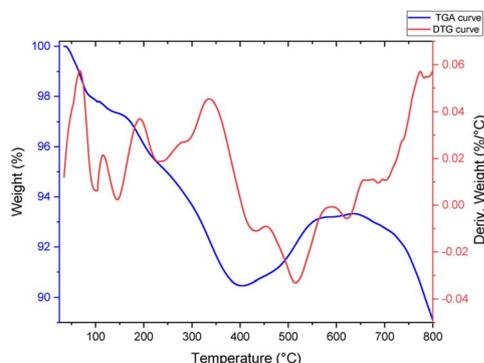
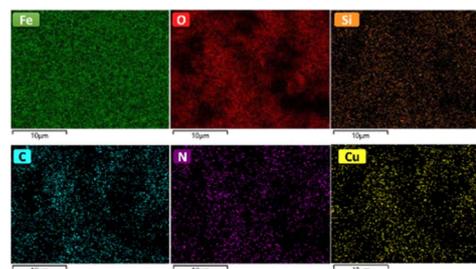**Fig. 3** TGA-DTG curves of the [Fe_3O_4@TAM-Schiff-base-Cu$^{(II)}$] complex.

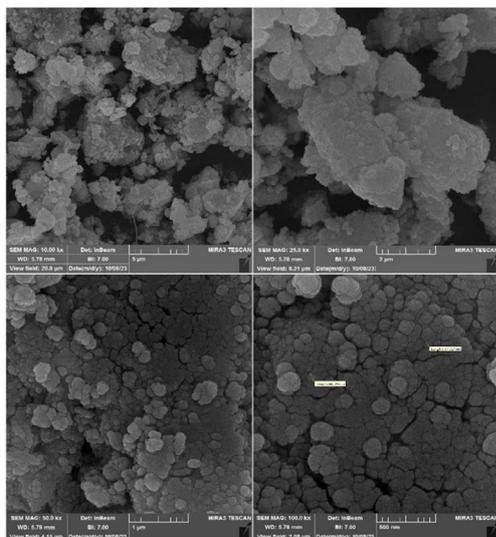**Fig. 5** Elemental mapping analysis of the [Fe_3O_4@TAM-Schiff-base-Cu$^{(II)}$] complex.

Fig. 6 SEM images of the [Fe_3O_4@TAM–Schiff-base–Cu$^{(II)}$] complex.

Fig. 8 VSM analysis of [Fe_3O_4@TAM–Schiff-base–Cu$^{(II)}$] complex.
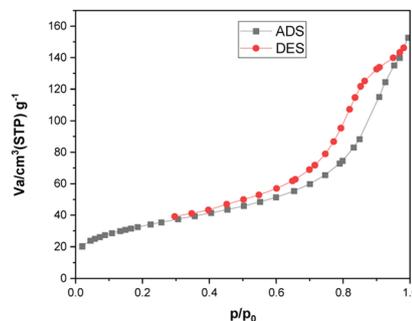
Fig. 9 N_2 adsorption–desorption isotherms of [Fe_3O_4@TAM–Schiff-base–Cu$^{(II)}$] complex.

nanoparticles with a uniform spherical shape. The average size of the particles was 25 nm, and more than 90% of them had a size in the range 9–18 nm (Fig. 7). The particle size is much bigger than that expected from Fe_3O_4 nanoparticles. As can be seen, there is a lighter shell with an amorphous structure and a dark crystalline magnetite core inside that suggests the formation of a core–shell structure. This suggests that a uniform layer of the [TAM-Schiff-base–Cu$^{(II)}$] complex was successfully immobilized on its surface, which caused some agglomerations on the outside of the Fe_3O_4 MNPs.

Value stream mapping (VSM)

The magnetic properties of the [Fe_3O_4@TAM-Schiff-base–Cu$^{(II)}$] complex were examined using VSM analysis (Fig. 8). The satisfaction magnetization value (MS value) was measured to be 44.92 emu g^{-1}. As compared to the bare Fe_3O_4 MS value,[56] it was revealed that the presence of the [TAM-Schiff-base–Cu$^{(II)}$] complex leads to a significant effect on the catalytic support. Keeping in mind that the ligand and linker components are diamagnetic in nature and decrease the MS value, it is worth mentioning that the elemental Cu$^{(II)}$ is paramagnetic because of the necessity of unpaired electrons in their orbitals (configuration is [Ar]3 d^9) and increases the MS value of the final complex.[57] Nevertheless, the super magnetic properties and high MS value of the [Fe_3O_4@TAM-Schiff-base–Cu$^{(II)}$] complex

Fig. 7 TEM images of the [Fe_3O_4@TAM-Schiff-base–Cu$^{(II)}$] complex.

meant that it could be easily isolated from the reaction mixture with the application of a simple external magnet.

Fig. 9 displays the N_2 adsorption–desorption isotherm of the [Fe_3O_4@TAM-Schiff-base–Cu$^{(II)}$] complex. As can be observed, the prepared nanostructure exhibits a Type IV isotherm, in line with the IUPAC classification for micro-mesoporous materials. These nanoparticles possess a specific surface area of 121.03 m^2 g^{-1}, a mean pore diameter of 7.6941 nm, and a total pore volume ($p/p_0 = 0.990$) of 0.2328 cm^3 g^{-1}. These characteristics play a significant role in enhancing its catalytic efficiency.

Catalytic studies

Optimization of reaction parameters

Regarding the green chemistry aspects and conditions in organic synthesis, herein we report the application of PEG-400 as a greener alternative to the traditional solvent in synthesizing the -substituted-1H-tetrazoles using the [Fe_3O_4@TAM-Schiff-base–Cu$^{(II)}$] complex as heterogeneous Lewis acid catalyst. Initially, the click reaction of benzonitrile and sodium azide was studied at 120 °C using PEG-400 media in a catalyst-free manner and in the presence of $FeCl_2 \cdot 4H_2O$, $FeCl_3 \cdot 6H_2O$, Fe_3O_4 and $Cu(NO_3)_2 \cdot 3H_2O$ salt as the catalyst. Accordingly, it was found out that the reactions required long times with a trace or minimum yields of product and the remaining benzonitrile reactant intact (TLC-based analysis). Afterwards, we varied the reaction conditions using various amounts of [Fe_3O_4@TAM-Schiff-base–Cu$^{(II)}$] and, accordingly, the best yield was obtained using 25 mg of catalyst. In a control experiment, an increase in

Table 1 Evaluation of reaction parameters on the synthesis of 5-phenyl-1H-tetrazole over the catalysis of the [Fe$_3$O$_4$@TAM-Schiff-base-Cu$^{(II)}$] complex
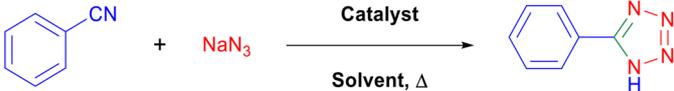
Entry	Catalyst	Catalyst (mg, (mol% of Cu))	Solvent	Temperature (°C)	Time (min)	Yield^{a,b} (%)	TON	TOF^c (min^{-1})
1	—	—	PEG	120	1 day	N.R	—	—
2	FeCl$_2$·4H$_2$O	25	PEG	120	95	N.R	—	—
3	FeCl$_3$·6H$_2$O	25	PEG	120	95	Trace	—	—
4	Fe$_3$O$_4$	25	PEG	120	95	11	57.89	0.60
5	Cu(NO$_3$)$_2$·3H$_2$O	25	PEG	120	95	15	78.94	0.83
6	[Fe$_3$O$_4$@TAM-Schiff-base-Cu$^{(II)}$] complex	20, (0.15)	PEG	120	240	73	486.66	2.02
7	[Fe$_3$O$_4$@TAM-Schiff-base-Cu$^{(II)}$] complex	25, (0.19)	PEG	120	100	98	515.78	5.16
8	[Fe$_3$O$_4$@TAM-Schiff-base-Cu$^{(II)}$] complex	35, (0.26)	PEG	120	95	97	373.07	3.93
9	[Fe$_3$O$_4$@TAM-Schiff-base-Cu$^{(II)}$] complex	50, (0.38)	PEG	120	85	98	257.89	3.03
10	[Fe$_3$O$_4$@TAM-Schiff-base-Cu$^{(II)}$] complex	25, (0.19)	DMSO	120	100	30	157.89	1.58
11	[Fe$_3$O$_4$@TAM-Schiff-base-Cu$^{(II)}$] complex	25, (0.19)	EtOH	Reflux	100	21	110.52	1.10
12	[Fe$_3$O$_4$@TAM-Schiff-base-Cu$^{(II)}$] complex	25, (0.19)	MeOH	Reflux	100	16	84.21	8.42
13	[Fe$_3$O$_4$@TAM-Schiff-base-Cu$^{(II)}$] complex	25, (0.19)	Acetone	Reflux	100	N.R	—	—
14	[Fe$_3$O$_4$@TAM-Schiff-base-Cu$^{(II)}$] complex	25, (0.19)	Ethyl acetate	Reflux	100	N.R	—	—
15	[Fe$_3$O$_4$@TAM-Schiff-base-Cu$^{(II)}$] complex	25, (0.19)	DI water	Reflux	100	41	215.78	2.16
16	[Fe$_3$O$_4$@TAM-Schiff-base-Cu$^{(II)}$] complex	25, (0.19)	PEG	100	170	96		
17	[Fe$_3$O$_4$@TAM-Schiff-base-Cu$^{(II)}$] complex	25, (0.19)	PEG	r.t	170	N.R	—	—

^{a} Isolated yield. ^{b} Conditions: benzonitrile (1 mmol), sodium azide (1.4 mmol), catalyst (mg) and solvent (1 mL). ^{c} The obtained values have been rounded to two decimal places.

the catalyst dose did not lead to an increment of the tetrazole adduct but resulted in a decrement of reaction time from 100 to 85 min, which indicates a decrease in the TOF of the catalyst. For further optimization purposes, we tried PEG-400, ethanol, methanol, water (as a protic-polar media), dimethyl sulfoxide, acetone, and ethyl acetate (as a non-protic media). In most cases, the reaction was not completed. Significantly, the best result was found with the PEG-400 solvent and, accordingly, it was selected as the optimal solvent. Finally, due to the versatile role of temperature on this transformation, we analyzed the effectiveness of it in various experimental conditions. It was observed that, when the reaction mixture was stirred at an elevated temperature (100 °C), the yield dropped while the reaction time increased to 170 min. Overall, all the observed results show that 25 mg of the [Fe$_3$O$_4$@TAM-Schiff-base-Cu$^{(II)}$] catalyst in PEG-400 at 120 °C is the optimal conditions for this process (Table 1).

Screening of reaction generality

Considering the ideal reaction conditions, we aimed at investigating the scope of the catalyst in click synthesis of different tetrazoles *via* replacing the benzonitrile with the substituted aromatic and aliphatic nitriles. Pleasingly, NaN$_3$ readily reacts with aryl nitriles having electron-withdrawing substituents to form the corresponding tetrazoles in excellent yields (Table 2). However, the aryl nitriles having electron-donating substituents, including chlorine, fluorine and hydroxyl groups at the

para and ortho positions, are less reactive as compared to the benzonitrile and aryl nitrile carrying electron-withdrawing nitro groups. Moreover, this is because of the fact that the increment of the negative charge on the nitrile group's carbon reduces the electrophilicity, which slows down their reaction with the N$_3^-$ agent. It is worth mentioning that the para substituent only contributes inductive and resonance effects whereas in the *ortho*-substituted one there is a strict hindrance too. Notably, aliphatic nitriles and Knoevenagel adducts, such as malononitrile, acetonitrile and 2-benzylmalononitrile, do not react with sodium azide, displaying no complementary products. These investigations show a high degree of selectivity for aromatic nitriles, which can be efficiently involved in the reaction and conversion to their corresponding tetrazole derivatives in presence of the [Fe$_3$O$_4$@TAM-Schiff-base-Cu$^{(II)}$] complex, while the aliphatic C≡N groups in the molecule will remain intact. Also, the nanocatalyst provides a good homoselectivity (Scheme 2) in dicyano-functional benzonitriles, such as phthalonitrile (Table 2, entry 12), for the synthesis of the corresponding tetrazoles (Scheme 3).

Reaction mechanism

The mechanism followed by the metal-based click synthesis of 5-aryl-1H-tetrazole derivatives is well described in our previously published articles.[16] As illustrated in Scheme 3, it begins with the interaction of Cu complex with a nitrile group – leading to the intermediate (I) R–C≡N–Cu$^{(III)}$. The second phase yields

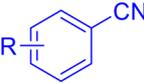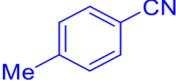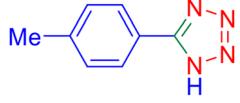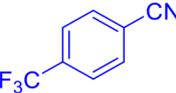**Table 2** The synthesis of 5-substituted 1H-tetrazoles over the catalysis of the [Fe$_3$O$_4$@TAM-Schiff-base-Cu$^{(II)}$] complex

Entry	Nitrile	Product	Time (min)	Yield[a,b] (%)	TON	TOF (min^{-1})	Melting point	
							Measured	Literature
1			100	98	515.78	5.16	215–217	211–214 (ref. 58)
2			220	93	489.47	2.45	249–251	252–254 (ref. 59)
3			70	96	505.26	7.21	221–222	218–219 (ref. 60)
4			150	98	515.78	3.43	145–146	149–152 (ref. 58)
5			120	93	489.47	4.07	219–220	217–220 (ref. 58)
6			270	95	500	1.85	157–159	158–160 (ref. 61)
7			300	93	489.47	1.63	179–180	180–181 (ref. 58)
8			150	94	494.73	3.29	252–254	261–263 (ref. 58)
9			280	96	505.26	1.80	264–266	264–266 (ref. 62)
10			35	97	510.52	14.58	223–224	224–226 (ref. 58)
11			80	95	500	6.25	234–236	233–235 (ref. 58)
12			65	94	494.73	7.611	211–213	209–211 (ref. 63)
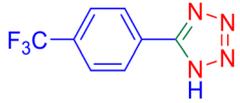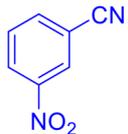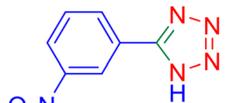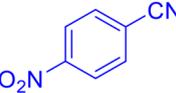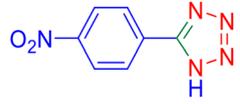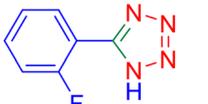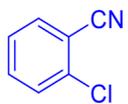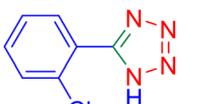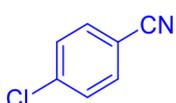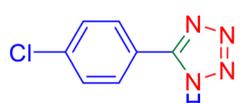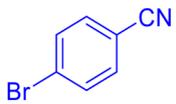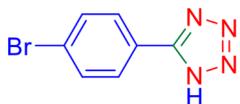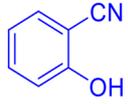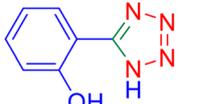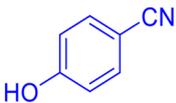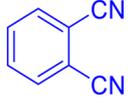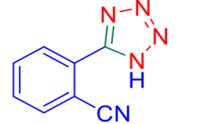
Table 2 (Contd.)

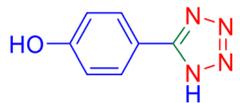| Entry | Nitrile | Product | Time (min) | Yield[a,b] (%) | TON | TOF (min⁻¹) | Melting point | |
							Measured	Literature
13			24 h	N.R	—	—	—	—
14			24 h	N.R	—	—	—	—
15			24 h	N.R	—	—	—	—

^{a} Isolated yield. ^{b} Conditions: aryl nitrile (1.0 mmol), sodium azide (1.4 mmol) and [Fe$_3$O$_4$@TAM-Schiff-base-Cu$^{(II)}$] complex (25 mg/0.175 mol%) in PEG-400 (1 mL) at 120 °C.
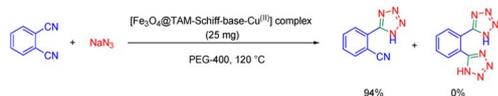
Scheme 2 Homoselectivity of the [Fe$_3$O$_4$@TAM-Schiff-base-Cu$^{(II)}$] complex in the synthesis of tetrazoles.
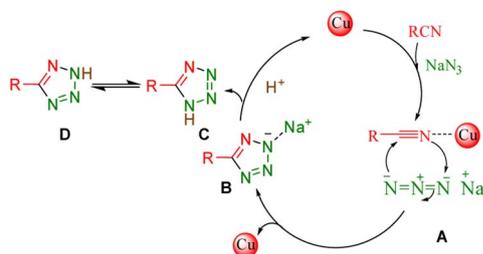
Scheme 3 Plausible mechanism for the click synthesis of 5-aryl-1H-tetrazoles over the catalysis of the [Fe$_3$O$_4$@TAM-Schiff-base-Cu(II)] complex.

intermediate (II) when the azide anion ($^-$N≡N$^+$ = N$^-$) attacks the R–C≡N–Cu$^{(III)}$ intermediate. Moreover, the Cu(II) catalyst with the appropriate lower oxidation state is regenerated when the resultant species is reduced. Finally, the corresponding 5-aryl-1H-tetrazole product is produced *via* an easy protonation of the anionic intermediate and acidifying the reaction using 10 mL of 4N.

Recyclability and hot filtration tests

The ability of the environmentally friendly catalysts to be recycled is one of the most noticeable features that distinguishes

them from conventional catalysts. In fact, it is necessary to verify the reusability of a new catalyst in order to avoid understating the cycle stability and operational applicability of the catalyst. In this regard, a study was conducted to investigate the [Fe$_3$O$_4$@TAM-Schiff-base-Cu(II)] recyclability on the model reaction. After the reaction was completed, the heterogeneous catalytic complex was separated using an external magnet, and then washed with hot water and ethanol. The recovered catalyst was then used in the next cycle of the reaction (Table 3). As shown in Fig. 10, it has been demonstrated that the [Fe$_3$O$_4$@-TAM-Schiff-base-Cu(II)] complex was able to be recovered and reused for four continuous cycles without significant loss of its capacity to catalyze the studied transformations or suffering a high loss in performance. FT-IR spectroscopy was performed on the recovered catalyst after 4 runs (Fig. 11). This analysis clearly indicated the presence of bands similar to those of the fresh catalyst. In addition, the N$_2$ adsorption–desorption isotherm of the reused catalyst is provided in Fig. 12. The result shows that the specific surface area was decreased to 38.533 m^2 g^{-1} that could be due to the accumulation of substrates on its surface.

Hot-filtration and leaching test

Hot filtration and leaching experiments were carried out on the model reaction. After 50 minutes, the heating was stopped, the reaction was diluted using hot water, and the catalytically active particles were removed *via* magnetic filtration. Furthermore, the filtrate was reintroduced into the oil bath and allowed to react for another 50 minutes. It was observed that the product yield did not considerably rise by more than 43%. In addition, the recovered catalyst was also studied applying ICP-AES

Table 3 Comparison of the catalytic efficiency of the [Fe₃O₄@TAM-Schiff-base-Cu$^{(II)}$] complex in a model reaction of the synthesis of 5-aryl-1H-tetrazole

Entry	Synthesis	Catalyst	Time (min)	Yield^{a} (%)	Ref.
1	5-Phenyl-1H-tetrazole	Boehmite@SiO₂@Tris-Cu(I)	120	95	58
2	5-Phenyl-1H-tetrazole	BNPs @SiO₂-TPPTSA	60	96	64
3	5-Phenyl-1H-tetrazole	Cu-Amd-RGO	30	96	65
4	5-Phenyl-1H-tetrazole	SA-rGO	240	94	66
5	5-Phenyl-1H-tetrazole	Fe₃O₄@SiO₂@BHA-Cu(II)	70	95	67
6	5-Phenyl-1H-tetrazole	[Fe₃O₄@TAM-Schiff-base-Cu$^{(II)}$] complex	100	98	This work

^{a} Isolated yield.
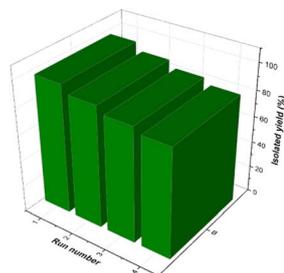
Fig. 10 Reusability of synthesized the [Fe₃O₄@TAM-Schiff-base-Cu$^{(II)}$] complex during the model reaction.
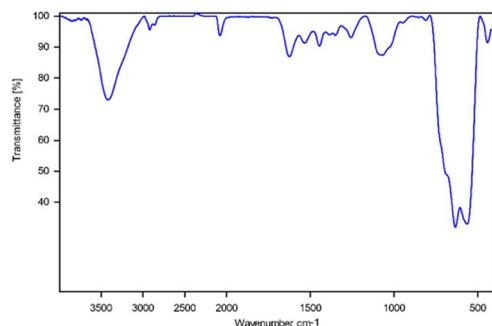
Fig. 11 FT-IR spectra of the [Fe₃O₄@TAM-Schiff-base-Cu$^{(II)}$] complex after four times of reuse.

Fig. 12 N₂ adsorption–desorption isotherms of the [Fe₃O₄@TAM-Schiff-base-Cu$^{(II)}$] complex after four times reuse.

analysis to quantify the copper leaching content (0.064 mmol g^{-1}). These observations demonstrate that the catalyst [Fe₃O₄@TAM-Schiff-base-Cu$^{(II)}$] is heterogeneous in nature.

Comparison

Considering Table 3, the results of the click synthesis of 5-aryl-1H-tetrazole in the presence of the [Fe₃O₄@TAM-Schiff-base-Cu$^{(II)}$] complex are compared to those of other transition metal-containing catalysts found in the literature. According to the comparative overview, [Fe₃O₄@TAM-Schiff-base-Cu$^{(II)}$] has one of the highest yields ever reported. This might be the consequence of a careful post-synthesis modification which includes the use of an acac-based tetraaza (N4 donor) macrocyclic Schiff base as an N-rich organic ligand to modify the electrical properties of the support, leading to an increment in the Cu ions

capacity to catalyze this click-type of reaction. It is noticeable that the [Fe₃O₄@TAM-Schiff-base-Cu$^{(II)}$] complex in which PEG-400 was used as a green solvent needed less reaction time and produced excellent yields, as compared to the listed approaches.

Conclusion

In conclusion, a straightforward technique has been designed to produce a novel nanomagnetic tetra-aza macrocyclic Schiff base complex of copper(II) as a powerful catalyst for the click reaction between aryl nitriles and NaN₃ in PEG-400 as an environmentally friendly solvent. This method selectively converts the aryl nitriles into the corresponding 5-aryl-1H-tetrazoles while the aliphatic nitriles remain intact. The performance of the homogeneous catalysis system remains consistent over four recycling cycles.

Data availability

The authors declare that all the data in this manuscript are available upon request.

Author contributions

M. N. supervised this work. N. M. conducted the experiments; M. M. did the data analysis and interpretation. All the authors discussed the results.

Conflicts of interest

The authors declare that they have no competing interests.

Acknowledgements

Notes and references

1 S. Pawar, M. K. Kumawat, M. Kundu and K. Kumar, Synthetic and Medicinal Perspective of Antileishmanial Agents: An Overview, *J. Mol. Struct.*, 2023, **1271**, 133977.

2 M. Farajpour, S. M. Vahdat, S. M. Baghbanian and M. Hatami, Ag-SiO$_2$ Nanoparticles: Benign, Expedient, and Facile Nano Catalyst in Synthesis of Decahydroacridines, *Chem. Methodol.*, 2023, **7**, 540–551.

3 L. V. Chanu and O. M. Singh, Recent Progress in the Synthesis of Azoles and Related Five-Membered Ring Heterocycles Using Silica-Supported Heterogeneous Catalysts, *J. Heterocycl. Chem.*, 2021, **58**, 2207–2225.

4 R. Muslim Muhiebes, L. Fatolahi and S. Sajjadifar, L-Proline Catalyzed Multicomponent Reaction for Simple and Efficient Synthesis of Tetrahydropyridines Derivatives, *Asian J. Green Chem.*, 2023, **7**, 121–131.

5 C. C. Eze, A. M. Ezeokonkwo, I. D. Ugwu, U. F. Eze, E. L. Onyeyilim, I. S. Attah and I. V. Okonkwo, Azole-Pyrimidine Hybrid Anticancer Agents: A Review of Molecular Structure, Structure Activity Relationship, and Molecular Docking, *Anticancer. Agents Med. Chem.*, 2022, **22**, 2822–2851.

6 M. Nasrollahzadeh, Z. Nezafat, N. S. S. Bidgoli and N. Shafiei, Use of Tetrazoles in Catalysis and Energetic Applications: Recent Developments, *Mol. Catal.*, 2021, **513**, 111788.

7 M. Nasrollahzadeh, M. Sajjadi, H. Ghafuri, N. S. S. Bidgoli, A. J. L. Pombeiro and S. Hazra, Platinum and Palladium Complexes with Tetrazole Ligands: Synthesis, Structure and Applications, *Coord. Chem. Rev.*, 2021, **446**, 214132.

8 S. Manzoor, Q. Tariq, X. Yin and J.-G. Zhang, Nitro-Tetrazole Based High Performing Explosives: Recent Overview of Synthesis and Energetic Properties, *Def. Technol.*, 2021, **17**, 1995–2010.

9 K. Ishihara, K. Ishihara, Y. Tanaka, T. Shioiri and M. Matsugi, Practical Synthesis of Tetrazoles from Amides and Phosphorazidates in the Presence of Aromatic Bases, *Tetrahedron*, 2022, **108**, 132642.

10 R. J. Herr, 5-Substituted-1H-Tetrazoles as Carboxylic Acid Isosteres: Medicinal Chemistry and Synthetic Methods, *Bioorganic Med. Chem.*, 2002, **10**, 3379–3393.

11 S. V. Voitekhovich, O. A. Ivashkevich and P. N. Gaponik, Synthesis, Properties, and Structure of Tetrazoles: Certain Achievements and Prospects, *Russ. J. Org. Chem.*, 2013, **49**, 635–654.

12 G. Aromí, L. A. Barrios, O. Roubeau and P. Gamez, Triazoles and Tetrazoles: Prime Ligands to Generate Remarkable Coordination Materials, *Coord. Chem. Rev.*, 2011, **255**, 485–546.

13 O. Savych, Y. O. Kuchkovska, A. V. Bogolyubsky, A. I. Konovets, K. E. Gubina, S. E. Pipko, A. V. Zhemera, A. V. Grishchenko, D. N. Khomenko, V. S. Brovarets, R. Doroschuk, Y. S. Moroz and O. O. Grygorenko, One-Pot Parallel Synthesis of 5-(Dialkylamino)Tetrazoles, *ACS Comb. Sci.*, 2019, **21**, 635–642.

14 C. G. Neochoritis, T. Zhao and A. Dömling, Tetrazoles via Multicomponent Reactions, *Chem. Rev.*, 2019, **119**, 1970–2042.

15 H. S. Lihumis, Z. A. Al Talebi and S. H. Shanan, Review on Role Alkyne and Azide Building Blocks for Click Chemistry in Organic Synthesis and Their Application, *Asian J. Green Chem.*, 2022, **6**, 68–87.

16 M. Koolivand, M. Nikoorazm, A. Ghorbani-Choghamarani and M. Mohammadi, A Novel Cubic Zn-citric Acid-based MOF as a Highly Efficient and Reusable Catalyst for the Synthesis of Pyranopyrazoles and 5-substituted 1H-tetrazoles, *Appl. Organomet. Chem.*, 2022, **36**, 2641–2663.

17 M. Mohammadi, M. Khodamorady, B. Tahmasbi, K. Bahrami and A. Ghorbani-Choghamarani, Boehmite Nanoparticles as Versatile Support for Organic–Inorganic Hybrid Materials: Synthesis, Functionalization, and Applications in Eco-Friendly Catalysis, *J. Ind. Eng. Chem.*, 2021, **97**, 1–78.

18 S. Swami, S. N. Sahu and R. Shrivastava, Nanomaterial Catalyzed Green Synthesis of Tetrazoles and Its Derivatives: A Review on Recent Advancements, *RSC Adv.*, 2021, **11**, 39058–39086.

19 S. Leyva-Ramos and J. Cardoso-Ortiz, Recent Developments in the Synthesis of Tetrazoles and Their Pharmacological Relevance, *Curr. Org. Chem.*, 2021, **25**, 388–403.

20 R. Mittal and S. K. Awasthi, Recent Advances in the Synthesis of 5-Substituted 1H-Tetrazoles: A Complete Survey (2013–2018), *Synth.*, 2019, **51**, 3765–3783.

21 M. Gao, L. Wang, Y. Yang, Y. Sun, X. Zhao and Y. Wan, Metal and Metal Oxide Supported on Ordered Mesoporous Carbon as Heterogeneous Catalysts, *ACS Catal.*, 2023, 4060–4090.

22 D. Wei, X. Shi, R. Qu, K. Junge, H. Junge and M. Beller, Toward a Hydrogen Economy: Development of Heterogeneous Catalysts for Chemical Hydrogen Storage and Release Reactions, *ACS Energy Lett.*, 2022, **7**, 3734–3752.

23 R. Mittal and S. K. Awasthi, Recent Advances in the Synthesis of 5-Substituted 1H-Tetrazoles: A Complete Survey (2013–2018), *Synthesis*, 2019, **51**, 3765–3783.

24 R. J. Herr, 5-Substituted-1H-Tetrazoles as Carboxylic Acid Isosteres: Medicinal Chemistry and Synthetic Methods, *Bioorg. Med. Chem.*, 2002, **10**, 3379–3393.

25 W. Jing, H. Shen, R. Qin, Q. Wu, K. Liu and N. Zheng, Surface and Interface Coordination Chemistry Learned from Model Heterogeneous Metal Nanocatalysts: From Atomically Dispersed Catalysts to Atomically Precise Clusters, *Chem. Rev.*, 2022, **123**, 5948–6002.

26 J. S. Bates, M. R. Johnson, F. Khamespanah, T. W. Root and S. S. Stahl, Heterogeneous M-N-C Catalysts for Aerobic

Oxidation Reactions: Lessons from Oxygen Reduction Electrocatalysts, *Chem. Rev.*, 2022, **123**, 6233–6256.

27 S. Feng, Y. Geng and H. L. H. Li, Targeted Intermetallic Nanocatalysts for Sustainable Biomass and CO 2 Valorization, *ACS Catal.*, 2022, **12**, 14999–15020.

28 J. Quinson, S. Kunz and M. Arenz, Surfactant-Free Colloidal Syntheses of Precious Metal Nanoparticles for Improved Catalysts, *ACS Catal.*, 2023, **13**, 4903–4937.

29 E. Opoku, Progress on Homogeneous Ruthenium Complexes for Water Oxidation Catalysis: Experimental and Computational Insights, *J. Chem. Rev.*, 2020, **2**, 211–227.

30 A. Ghorbani-Choghamarani, M. Mohammadi, L. Shiri and Z. Taherinia, Synthesis and Characterization of Spinel FeAl2O4 (Hercynite) Magnetic Nanoparticles and Their Application in Multicomponent Reactions, *Res. Chem. Intermed.*, 2019, **45**, 5705–5723.

31 R. Das, D. Mukherjee, S. Reja, K. Sarkar and A. Kejriwal, Copper Based N,N-Dimethyl-N-(1-Pyridinylmethylidene) Propane-1,3-Diamine Compound: Synthesis, Characterization, and Its Application toward Biocidal Activity, *J. Appl. Organomet. Chem.*, 2023, **3**, 73–85.

32 N. Pourbahar and S. Sattari Alamdar, Phytofabrication, and Characterization of Ag/Fe$_3$O$_4$ Nanocomposite from Rosa Canina Plant Extracts Using a Green Method, *Asian J. Green Chem.*, 2023, **7**, 9–16.

33 M. Norouzi and M. Khanmoradi, Brønsted-acidic ionic liquid supported nanomagnetic: a novel and reusable catalyst for synthesis of oxygen-containing heterocyclic compounds, *Res. Chem. Intermed.*, 2023, 1–20.

34 A. Mohsin, M. H. Hussain, M. Z. Mohsin, W. Q. Zaman, M. S. Aslam, A. Shan, Y. Dai, I. M. Khan, S. Niazi, Y. Zhuang and M. Guo, Recent Advances of Magnetic Nanomaterials for Bioimaging, Drug Delivery, and Cell Therapy, *ACS Appl. Nano Mater.*, 2022, **5**, 10118–10136.

35 Y. Kang, S. Shi, H. Sun, J. Dan, Y. Liang, Q. Zhang, Z. Su, J. Wang and W. Zhang, Magnetic Nanoseparation Technology for Efficient Control of Microorganisms and Toxins in Foods: A Review, *J. Agric. Food Chem.*, 2022, **70**, 16050–16068.

36 X. Zhong, Z. Li, R. Shi, L. Yan, Y. Zhu and H. Li, Schiff Base-Modified Nanomaterials for Ion Detection: A Review, *ACS Appl. Nano Mater.*, 2022, **5**, 13998–14020.

37 D. Esteban, D. Bañobre, R. Bastida, A. de Blas, A. Macías, A. Rodríguez, T. Rodríguez-Blas, D. E. Fenton, H. Adams and J. Mahía, Barium Templating Schiff-Base Lateral Macrobicycles, *Inorg. Chem.*, 1999, **38**, 1937–1944.

38 Y. Jia and J. Li, Molecular Assembly of Schiff Base Interactions: Construction and Application, *Chem. Rev.*, 2015, **115**, 1597–1621.

39 A. M. Hassan, A. O. Said, B. H. Heakal, A. Younis, W. M. Aboulthana and M. F. Mady, Green Synthesis, Characterization, Antimicrobial and Anticancer Screening of New Metal Complexes Incorporating Schiff Base, *ACS Omega*, 2022, **7**, 32418–32431.

40 F. Lam, J. X. Xu and K. S. Chan, Binucleating Ligands: Synthesis of Acyclic Achiral and Chiral Schiff Base–Pyridine and Schiff Base–Phosphine Ligands, *J. Org. Chem.*, 1996, **61**, 8414–8418.

41 S. J. Dorazio and J. R. Morrow, Iron(II) Complexes Containing Octadentate Tetraazamacrocycles as ParaCEST Magnetic Resonance Imaging Contrast Agents, *Inorg. Chem.*, 2012, **51**, 7448–7450.

42 T. J. Hubin, J. M. McCormick, N. W. Alcock, H. J. Clase and D. H. Busch, Crystallographic Characterization of Stepwise Changes in Ligand Conformations as Their Internal Topology Changes and Two Novel Cross-Bridged Tetraazamacrocyclic Copper(II) Complexes, *Inorg. Chem.*, 1999, **38**, 4435–4446.

43 C. A. Boswell, X. Sun, W. Niu, G. R. Weisman, E. H. Wong, A. L. Rheingold and C. J. Anderson, Comparative *in Vivo* Stability of Copper-64-Labeled Cross-Bridged and Conventional Tetraazamacrocyclic Complexes, *J. Med. Chem.*, 2004, **47**, 1465–1474.

44 P. V. Bernhardt and P. C. Sharpe, Structurally Reinforced Tetraazamacrocyclic Complexes, *Inorg. Chem.*, 2000, **39**, 2020–2025.

45 M. Azizi, S. Seidi and A. Rouhollahi, A Novel N,N′-Bis(Acetylacetone)Ethylenediimine Functionalized Silica-Core Shell Magnetic Nanosorbent for Magnetic Dispersive Solid Phase Extraction of Copper in Cereal and Water Samples, *Food Chem.*, 2018, **249**, 30–37.

46 D. Saberi, S. Mahdudi, S. Cheraghi and A. Heydari, Cu(II)–Acetylacetone Complex Covalently Anchored onto Magnetic Nanoparticles: Synthesis, Characterization and Catalytic Evaluation in Amide Bond Formation via Oxidative Coupling of Carboxylic Acids with *N,N*-Dialkylformamides, *J. Organomet. Chem.*, 2014, **772–773**, 222–228.

47 A. Ghorbani-Choghamarani, Z. Taherinia and M. Mohammadi, Facile Synthesis of Fe$_3$O$_4$@GlcA@Ni-MOF Composites as Environmentally Green Catalyst in Organic Reactions, *Environ. Technol. Innov.*, 2021, **24**, 102050.

48 M. Mohammadi and A. Ghorbani-Choghamarani, A Novel Hercynite-Supported Tetradentate Schiff Base Complex of Manganese Catalyzed One-Pot Annulation Reactions, *Appl. Organomet. Chem.*, 2022, **36**, e6905.

49 F. Ghobakhloo, D. Azarifar, M. Mohammadi and M. Ghaemi, γ-Fe$_2$O$_3$@Cu$_3$Al-LDH/HEPES a Novel Heterogeneous Amphoteric Catalyst for Synthesis of Annulated Pyrazolo [3,4-d]Pyrimidines, *Appl. Organomet. Chem.*, 2022, **36**, e6823.

50 F. Ghobakhloo, D. Azarifar, M. Mohammadi, H. Keypour and H. Zeynali, Copper(II) Schiff-Base Complex Modified UiO-66-NH2(Zr) Metal-Organic Framework Catalysts for Knoevenagel Condensation-Michael Addition-Cyclization Reactions, *Inorg. Chem.*, 2022, **61**, 4825–4841.

51 A. Ghorbani-Choghamarani, Z. Darvishnejad and M. Norouzi, Synthesis and Characterization of Copper(II) Schiff Base Complex Supported on Fe$_3$O$_4$ Magnetic Nanoparticles: A Recyclable Catalyst for the One-Pot Synthesis of 2,3-Dihydroquinazolin-4(1H)-Ones, *Appl. Organomet. Chem.*, 2015, **29**, 707–711.

52 M. Norouzi, A. Ghorbani-Choghamarani and M. Nikoorazm, Heterogeneous Cu(II)/L-His@Fe$_3$O$_4$ Nanocatalyst: A Novel, Efficient and Magnetically-Recoverable Catalyst for Organic

Transformations in Green Solvents, *RSC Adv.*, 2016, **6**, 92387–92401.

53 Z. Ali, L. Tian, P. Zhao, B. Zhang, A. Nisar, X. Li, H. Zhang and Q. Zhang, Micron-Sized Flower-like Fe_3O_4@GMA Magnetic Porous Microspheres for Lipase Immobilization, *RSC Adv.*, 2015, **5**, 92449–92455.

54 A. Ghorbani-Choghamarani and M. Norouzi, Suzuki, Stille and Heck Cross-Coupling Reactions Catalyzed by Fe_3O_4@PTA–Pd as a Recyclable and Efficient Nanocatalyst in Green Solvents, *New J. Chem.*, 2016, **40**, 6299–6307.

55 B. Thangaraj, Z. Jia, L. Dai, D. Liu and W. Du, Lipase NS81006 Immobilized on Fe_3O_4 Magnetic Nanoparticles for Biodiesel Production, *Ovidius Univ. Ann. Chem.*, 2016, **27**, 13–21.

56 A. Ghorbani-Choghamarani and M. Norouzi, Palladium Supported on Modified Magnetic Nanoparticles: A Phosphine-Free and Heterogeneous Catalyst for Suzuki and Stille Reactions, *Appl. Organomet. Chem.*, 2016, **30**, 140–147.

57 M. Mohammadi, A. Ghorbani-Choghamarani and N. Hussain-Khil, L-Aspartic Acid Chelan–Cu(II) Complex Coted on $ZrFe_2O_4$ MNPs Catalyzed One–Pot Annulation and Cooperative Geminal-Vinylogous Anomeric–Based Oxidation Reactions, *J. Phys. Chem. Solids*, 2023, **177**, 111300.

58 A. Ghorbani-Choghamarani, H. Aghavandi and M. Mohammadi, Boehmite@SiO_2@Tris(Hydroxymethyl) Aminomethane-Cu(I): A Novel, Highly Efficient and Reusable Nanocatalyst for the C-C Bond Formation and the Synthesis of 5-substituted 1H-tetrazoles in Green Media, *Appl. Organomet. Chem.*, 2020, **34**, e5804.

59 A. Najafi Chermahini, N. \. Andisheh and A. Teimouri, KIT-6-Anchored Sulfonic Acid Groups as a Heterogeneous Solid Acid Catalyst for the Synthesis of Aryl Tetrazoles, *J. Iran. Chem. Soc.*, 2018, **15**, 831–838.

60 R. Jiang, H. Sun Bin, S. Li, K. Zhan, J. Zhou, L. Liu, K. Zhang, Q. Liang and Z. Chen, Synthesis of Tetrazoles, Triazoles, and Imidazolines Catalyzed by Magnetic Silica Spheres Grafted Acid, *Synth. Commun.*, 2018, **48**, 2652–2662.

61 S. Paudel, X. Min, S. Acharya, D. B. Khadka, G. Yoon, K. M. Kim and S. H. Cheon, Triple Reuptake Inhibitors: Design, Synthesis and Structure–Activity Relationship of Benzylpiperidine–Tetrazoles, *Bioorganic Med. Chem.*, 2017, **25**, 5278–5289.

62 N. Nowrouzi, S. Farahi and M. Irajzadeh, 4-(N,N-Dimethylamino)Pyridinium Acetate as a Recyclable Catalyst for the Synthesis of 5-Substituted-1H-Tetrazoles, *Tetrahedron Lett.*, 2015, **56**, 739–742.

63 M. Nikoorazm, B. Tahmasbi, S. Gholami and P. Moradi, Copper and Nickel Immobilized on Cytosine@MCM-41: As Highly Efficient, Reusable and Organic–Inorganic Hybrid Nanocatalysts for the Homoselective Synthesis of Tetrazoles and Pyranopyrazoles, *Appl. Organomet. Chem.*, 2020, **34**, e5919.

64 M. Khodamorady, N. Ghobadi and K. Bahrami, Homoselective Synthesis of 5-Substituted 1H-Tetrazoles and One-Pot Synthesis of 2,4,5-Trisubstituted Imidazole Compounds Using BNPs@SiO_2-TPPTSA as a Stable and New Reusable Nanocatalyst, *Appl. Organomet. Chem.*, 2021, **35**, e6144.

65 P. A. Kulkarni, A. K. Satpati, M. Thandavarayan and S. S. Shendage, An Efficient Cu/Functionalized Graphene Oxide Catalyst for Synthesis of 5-Substituted 1H-Tetrazoles, *Chem. Pap.*, 2021, **75**, 2891–2899.

66 R. Mittal, A. Kumar and S. K. Awasthi, Practical Scale up Synthesis of Carboxylic Acids and Their Bioisosteres 5-Substituted-1H-Tetrazoles Catalyzed by a Graphene Oxide-Based Solid Acid Carbocatalyst, *RSC Adv.*, 2021, **11**, 11166–11176.

67 M. Norouzi and S. Beiranvand, Fe_3O_4@SiO_2@BHA-Cu(II) as a new, effective, and magnetically recoverable catalyst for the synthesis of polyhydroquinoline and tetrazole derivatives, *J. Chem. Sci.*, 2023, **135**, 1–13.